Supporting Information

Macroscopic Strain-Induced Transition from Quasi-Infinite Gold Nanoparticle Chains to Defined Plasmonic Oligomers

Anja Maria Steiner,[1] Martin Mayer,[1,2] Maximilian Seuss,[1]
Svetoslav Nikolov,[3] Kenneth D. Harris,[1,4] Alexander Alexeev,[3]
Christian Kuttner,[1,2,*] Tobias A.F. König,[1,2,*] and Andreas Fery[1,2,5,*]

[1]Leibniz-Institut für Polymerforschung Dresden e.V., Institute of Physical Chemistry and Polymer Physics, Hohe Str. 6, 01069 Dresden, Germany

[2]Cluster of Excellence Centre for Advancing Electronics Dresden (cfaed), Technische Universität Dresden, 01062 Dresden, Germany

[3]George W. Woodruff School of Mechanical Engineering, Georgia Institute of Technology, 771 Ferst Drive NW., Atlanta, Georgia 30332, United States

[4]National Institute for Nanotechnology, 11421 Saskatchewan Drive, Edmonton, AB, Canada

[5]Department of Physical Chemistry of Polymeric Materials, Technische Universität Dresden, Hohe Str. 6, 01069 Dresden, Germany

Corresponding Authors:

*C.K.: kuttner@ipfdd.de, *T.A.F.K.: koenig@ipfdd.de, *A.F.: fery@ipfdd.de

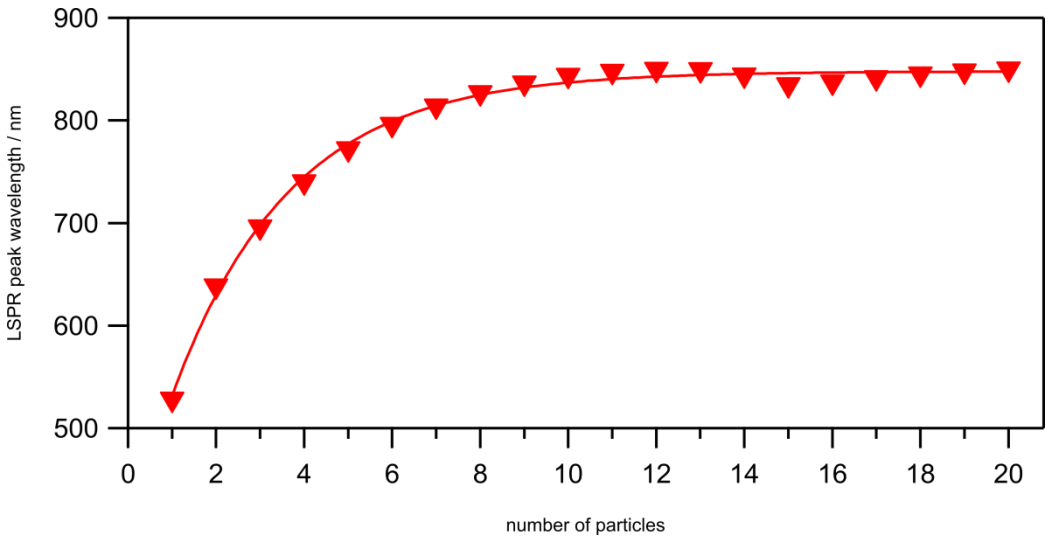

Figure S1: Identification of the infinite chain limit for 70 nm gold nanoparticles with 2 nm inter-particle distance. The position of the longitudinal surface plasmon resonance for isolated plasmonic oligomers of continuously increasing numbers of particles was simulated by generalized multiparticle Mie theory (GMMT). At approximately 10 particles, the longitudinal superradiant mode stabilizes and shifts to longer wavelengths become negligible. Thus, above this “infinite chain limit”, the assembly behaves like an infinite particle chain and can be described as a plasmonic polymer.

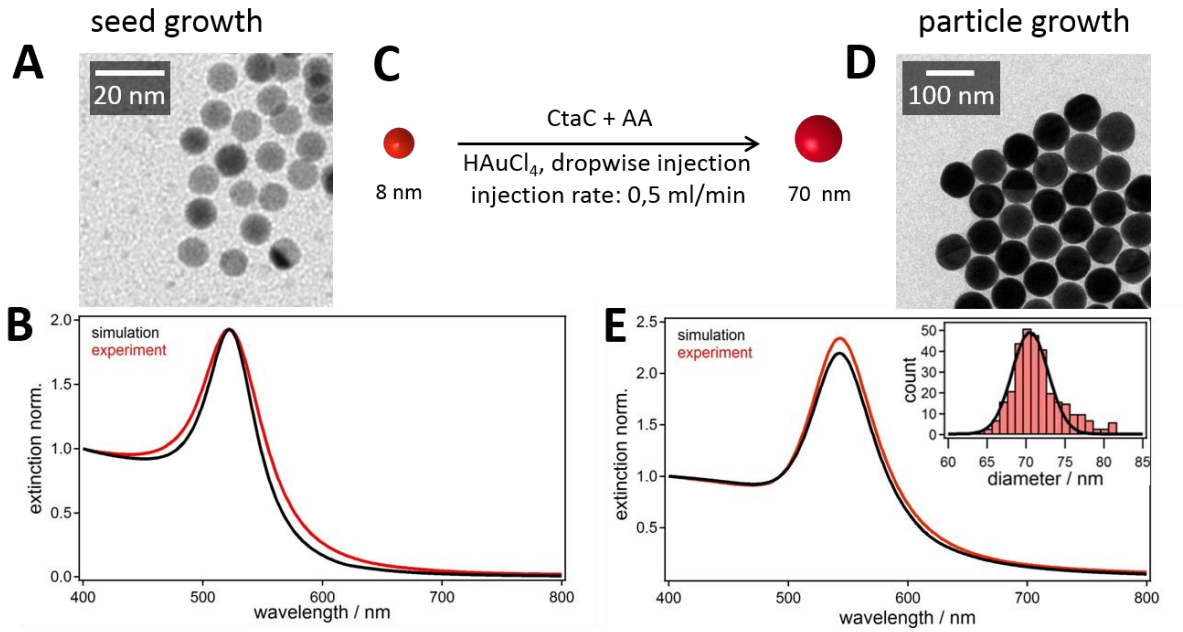

Figure S2: Seed-mediated growth of narrowly distributed gold nanospheres. Spherical particles with a diameter of 8 nm were synthesized *via* a one-shot seeded reaction using Wulff particles as seeds. Characterization by TEM (**A**) and correlation of experimental and simulated extinction spectra (**B**) suggest highly spherical particles with a narrow size distribution. The as-prepared 8 nm particles were used as seeds for the next overgrowth step, illustrated schematically in **C**. Analysis of TEM images (**D**) for 350 particles (**E, inset**) yielded an average diameter of 70.5 ± 1.2 nm. Experimentally determined extinction spectra (**E, red**) match Mie simulations (**black**).

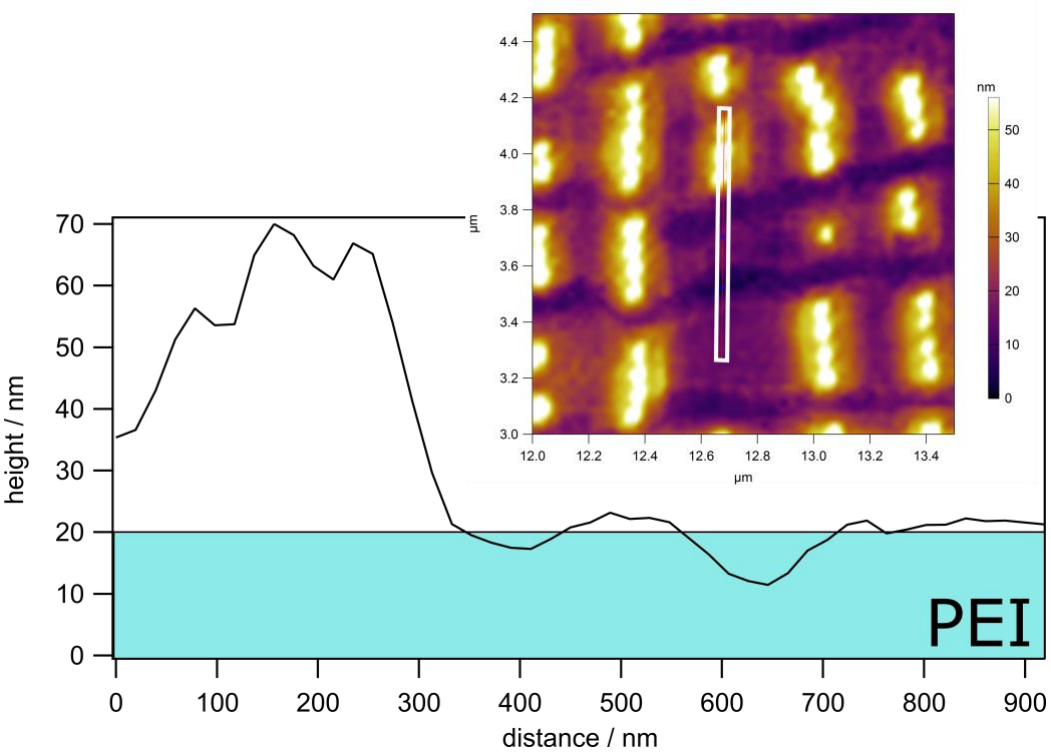

Figure S3: Determination of the embedding depth for 70 nm particles in the PEI adhesion layer. The location of the line-profile is highlighted in the AFM image in white color. Taking the size of the nanoparticle into account, the depth of embedding can be estimated to be approx. 20 nm.

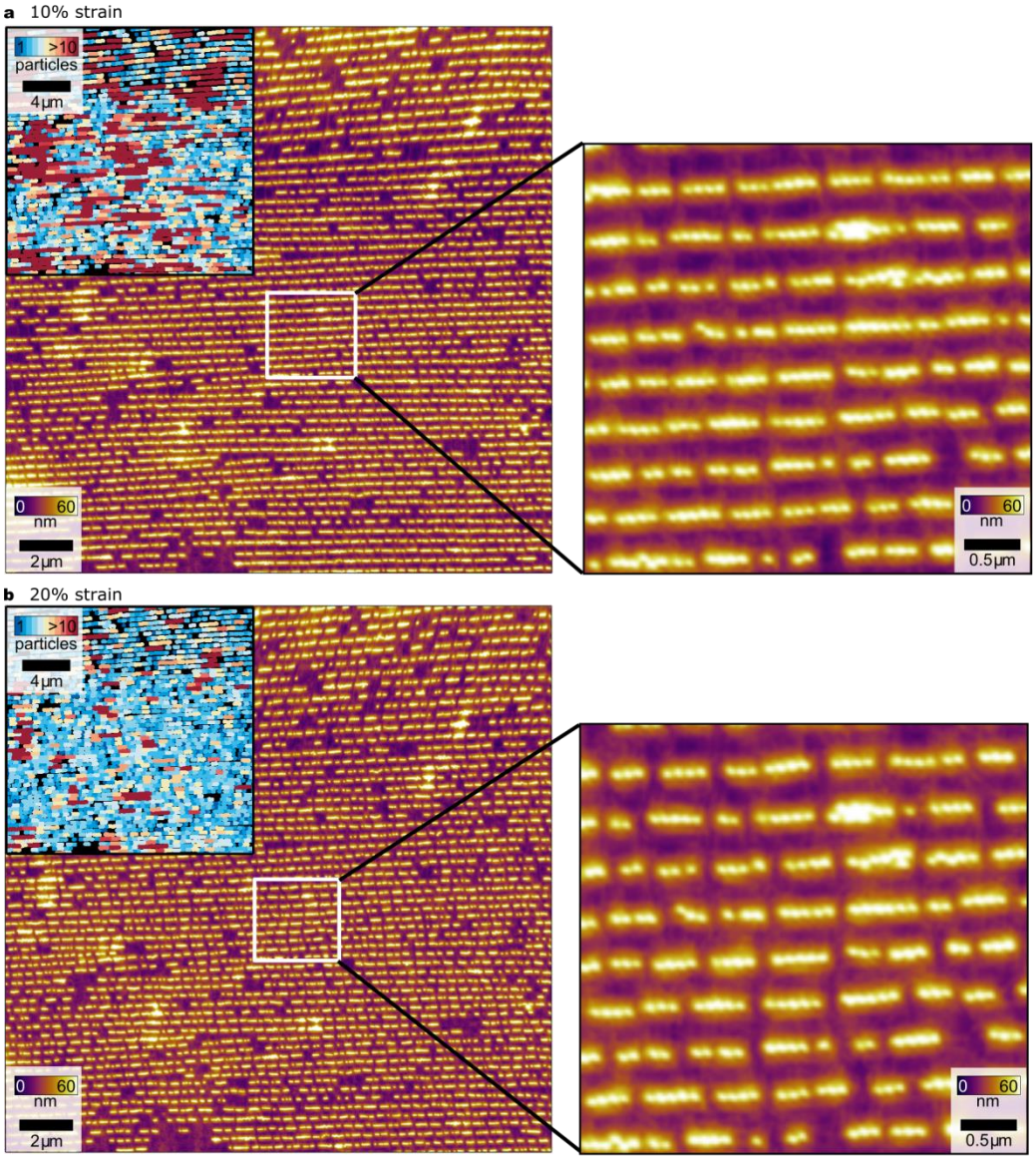

Figure S4: Morphological characterization *via in-situ* AFM imaging at intermediate strains. Height images at 10% (**a**), and 20% (**b**) strain at low magnification (**left**) and higher magnification (**right**), which allow individual nanoparticles to be distinguished. In the **insets (left),** the lengths of the individual chains are illustrated by false colors (longer chains, red; shorter chains, blue). See **Fig. S8** for details about the evaluation.

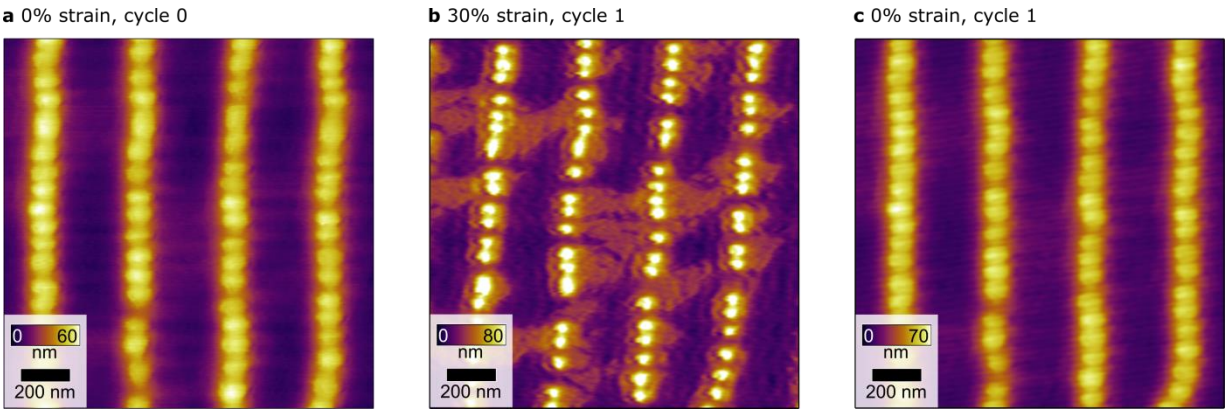

Figure S5: Reversibility Measurements via same-spot AFM Imaging. Height images of the initial state at 0% strain (**a**), the stretches state at 30% strain (**b**) and the released substrate without applied strain (**c**) show complete reversibility.

S1 Mechanical modeling by the lattice spring method

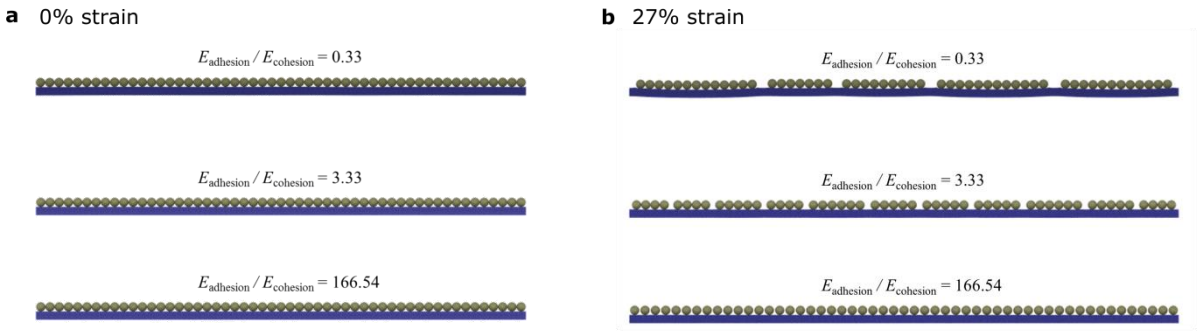

Figure S6: Mechanical simulations by lattice spring modeling: Fragmentation of quasi-infinite particle chains with different ratios of particle-substrate adhesion to interparticle cohesion forces. **(a)** 0% strain, **(b)** 27% strain (see **Video S1**)**.**

In the computational model, the PDMS surface was represented using the lattice spring method (LSM),[1] which is a lattice-based technique for modeling elastic solids. To construct the substrate, we used a simple cubic lattice with dimensions of 20.5 x 9.5 x *Z* lattice units. Three values of Z were considered, 850.5, 567, and 283.5, corresponding to 81, 53, and 27 gold nanoparticles, respectively. The lattice spacing was set equal to 0.5 lattice units. The nanoparticles, with outer diameters of 10 lattice units, were modeled using a collection of beads, which were positioned at nodal locations in a spherical mesh. The surface mesh was generated using Delaunay triangulation with a force-based smoothing procedure.[2] Each nanoparticle was represented by 1,320 beads. To simulate the cohesive interactions between the nanoparticles, we utilized the following Morse potential:

$$E(r) = D \cdot \left[e^{-2\,\alpha(r-r_0)} - 2\,e^{-\alpha\,(r-r_0)} \right] \qquad \textbf{eq. S1}$$

To set the initial equilibrium spacing between neighboring nanoparticles to approximately 0.5 lattice units, the distance cutoff of the Morse potential was set to 1.5 lattice units. The scaling constant α was set to 3.75 inverse. lattice units, and r_0 was set to 0.9 lattice units. The effect of thermal fluctuations was accounted for by the dissipative particle dynamics (DPD) thermostat with γ= 4.5, and a cutoff at 1.[3] The adhesive interactions between the nanoparticles and substrate were represented by harmonic bonds. The equilibrium length of the bonds was set to 0.5 lattice units to ensure a spacing of approximately 0.5 lattice units between the nanoparticle and the elastic substrate. Furthermore, a linear repulsive potential between the LSM nodes on the substrate and beads on the surface of the nanoparticles was included to prevent nanoparticle-substrate penetration. This linear potential was characterized by a cut-off distance of 0.5 lattice units and strength 100 energy units.

We characterize the cohesive forces in the simulations by defining $E_{cohesion}=D(A_{cap}/\delta)^2$, where D is the strength of the Morse potential, A_{cap} is the surface area of the spherical cap over which the Morse potential acts, and $\delta \approx 0.65$ is the particle spacing on the spherical shell. In the simulations, we varied D in the range from 0.5 to 500 energy units, whereas A_{cap}/δ was set constant. We estimated the adhesive energy as $E_{adhesion} = k\,N\,R^2$. Here, $N = 71$ is the number of bonds per bead, $k = 50$ is the spring stiffness in energy units per square lattice unit, and $R = 5$ is the nanoparticle radius in lattice units. The substrate has periodic boundaries in the x and z dimensions. Stretching in the z-direction is achieved by incrementally increasing the box length in the z dimension. Each strain step deforms the box a distance of 1 lattice unit. The final strain on the substrate was 27%. Viscous damping was applied to dissipate any oscillations in the model. The dissipative force was made proportional to the bead velocity, with a proportionality constant set to 0.1.

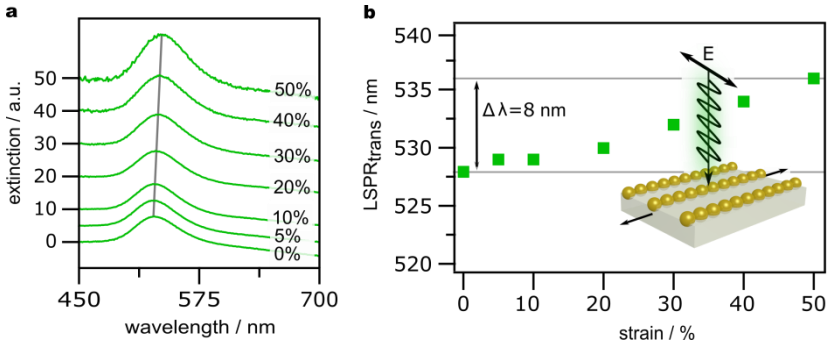

Figure S7: Strain-dependent UV-vis-NIR spectroscopy for transversal excitation. Upon stretching, extinction spectra (**a**) reveal a continuous linear red-shift of the LSPR position up to 8 nm between 0% and 50% strain. The observed shift (**b**) can be attributed to the reduction of energetically unfavorable transversal coupling within chain assemblies. Interline coupling can be neglected as the line spacing is always larger than five times the particle radius.[4] The Poisson's contraction which accompanies stretching is therefore insufficient to evoke plasmonic chain interactions (at the maximum 50% strain, the line spacing is 254 nm). This is in accordance with the distances determined by AFM measurements.

S2 Spectral deconvolution

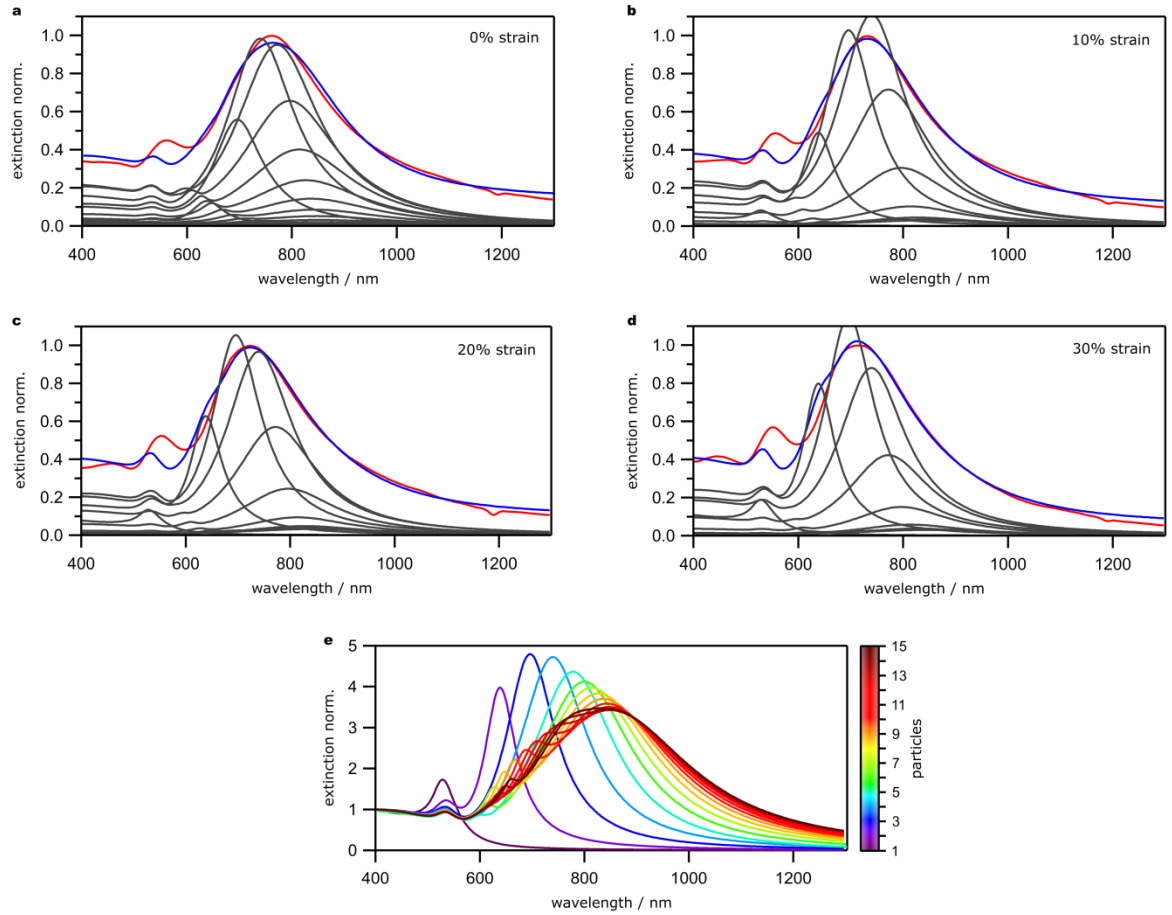

Figure S8: Deconvolution of experimental spectra (a–d, red) at varying strains (0%, 10%, 20%, and 30%). Histograms for the distribution of oligomer lengths were determined by deconvolution of the experimental extinction spectra. For this purpose, ideal extinction cross-sections of individual oligomers (**e**, 1–20 particles per chain) were calculated by GMMT.[5]

The isolated chains were modeled with uniform 2 nm interparticle distances and a surrounding medium with an effective refractive index of 1.2 to account for embedding in PEI. The deconvolution was performed by an Igor Pro 6 (Wavemetrics, USA) curve-fitting function, in which the ensemble-averaged extinction spectra (**blue**) were calculated on the basis of exponentially modified Gaussian distributions (ExpModGauss)[6] (see **eq. S2**) of the individual simulated extinction cross-sections (**gray**, weighted by the resulting distribution).

$$f(x;\mu,\sigma,\tau) = \frac{h\sigma}{\tau}\sqrt{\frac{\pi}{2}}\exp\left(\frac{1}{2}\left(\frac{\sigma}{\tau}\right)^2 - \frac{x-\mu}{\tau}\right)\operatorname{erfc}\left(\frac{1}{\sqrt{2}}\left(\frac{\sigma^2}{\tau} - \frac{x-\mu}{\sigma}\right)\right) \qquad \textbf{eq. S2}$$

$$\text{mean} = \mu + \tau \qquad \textbf{eq. S3}$$

$$\text{variance} = \sigma^2 + \tau^2 \qquad \textbf{eq. S4}$$

The ExpModGauss distributions *f(x)* were matched under consideration of the experimental AFM data. Here, *x* represents the aliquot of oligomers in the ensemble-averaged distribution. The fitting parameters μ, σ define the shape of the Gaussian, and τ controls the exponential modification. All fits converged properly without constrains. The mean value and the variance can be calculated by **eq. S3** and **eq**. **S4**, respectively.

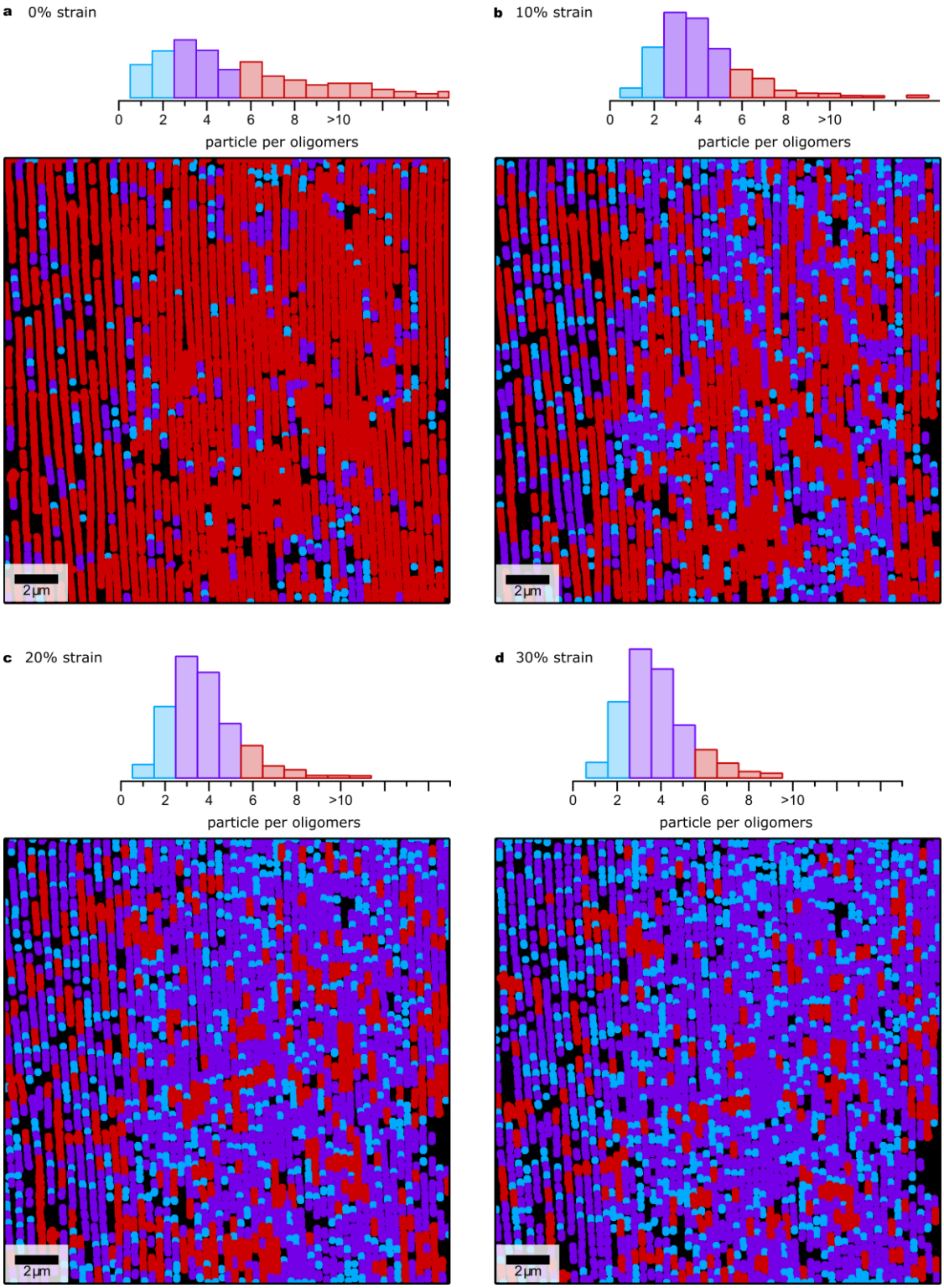

Figure S9: Graphical illustration of the chain length distributions evaluated by AFM analysis. The distributions of oligomers at the strains noted ($X_{N,AFM}$, **a–d, top**) are color-coded in the AFM images (**a–d, bottom**) based on the chain length: < 3 particles (**pale blue**), 3-5 particles (**purple**), and > 5 particles (**red**). This allows the breakup of long chains into defined oligomers to be tracked from 0% to 30% strain. Starting from predominantly quasi-infinite chains at zero strain, the distributions shifts toward shorter chains with narrower length distributions.

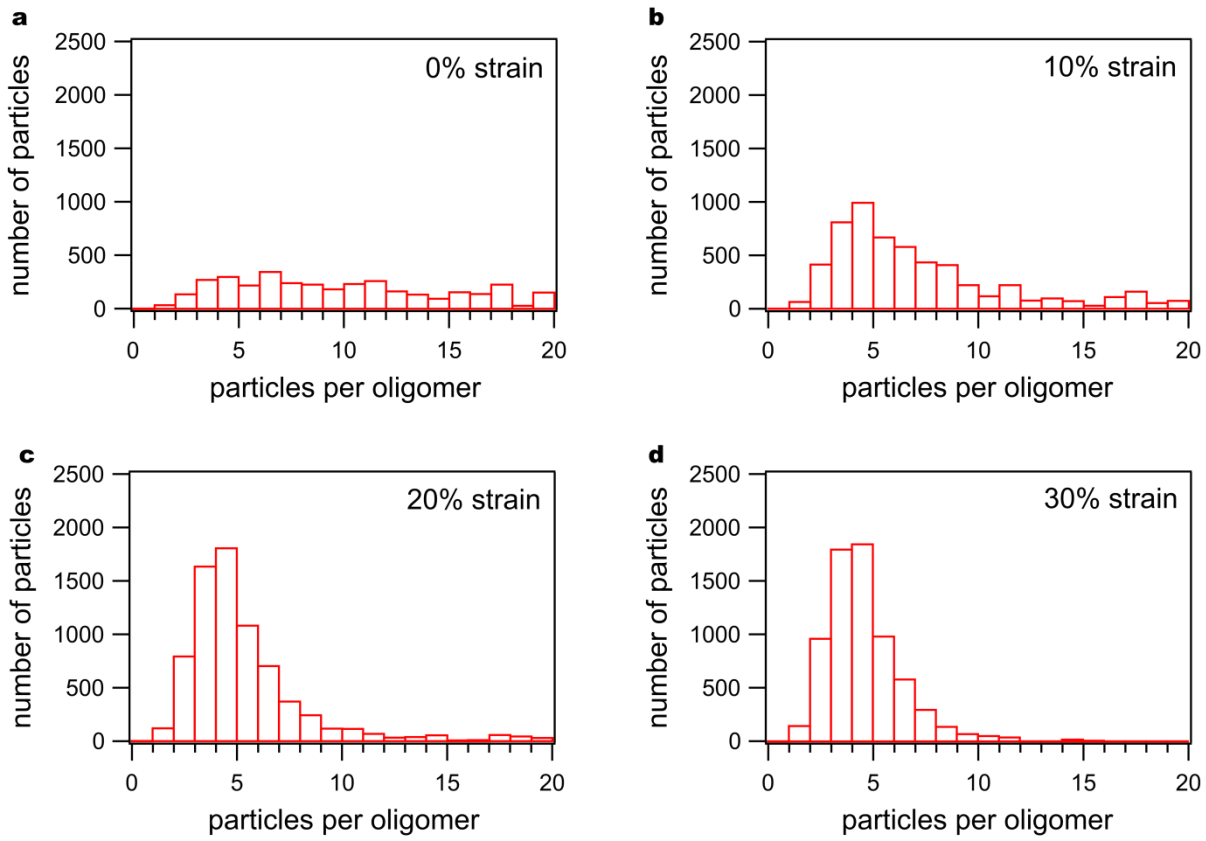

Figure S10: Evaluation of the oligomer distributions based on AFM data and weighted by the number of particles per oligomer ($X_{w,AFM}$). The distributions weighted by the number of oligomers ($X_{n,AFM}$) was calculated from the same data and used for the evaluation of the dispersity *Đ*, *i.e.,* the ensemble-averaged dispersity in length.

S3 AFM image analysis

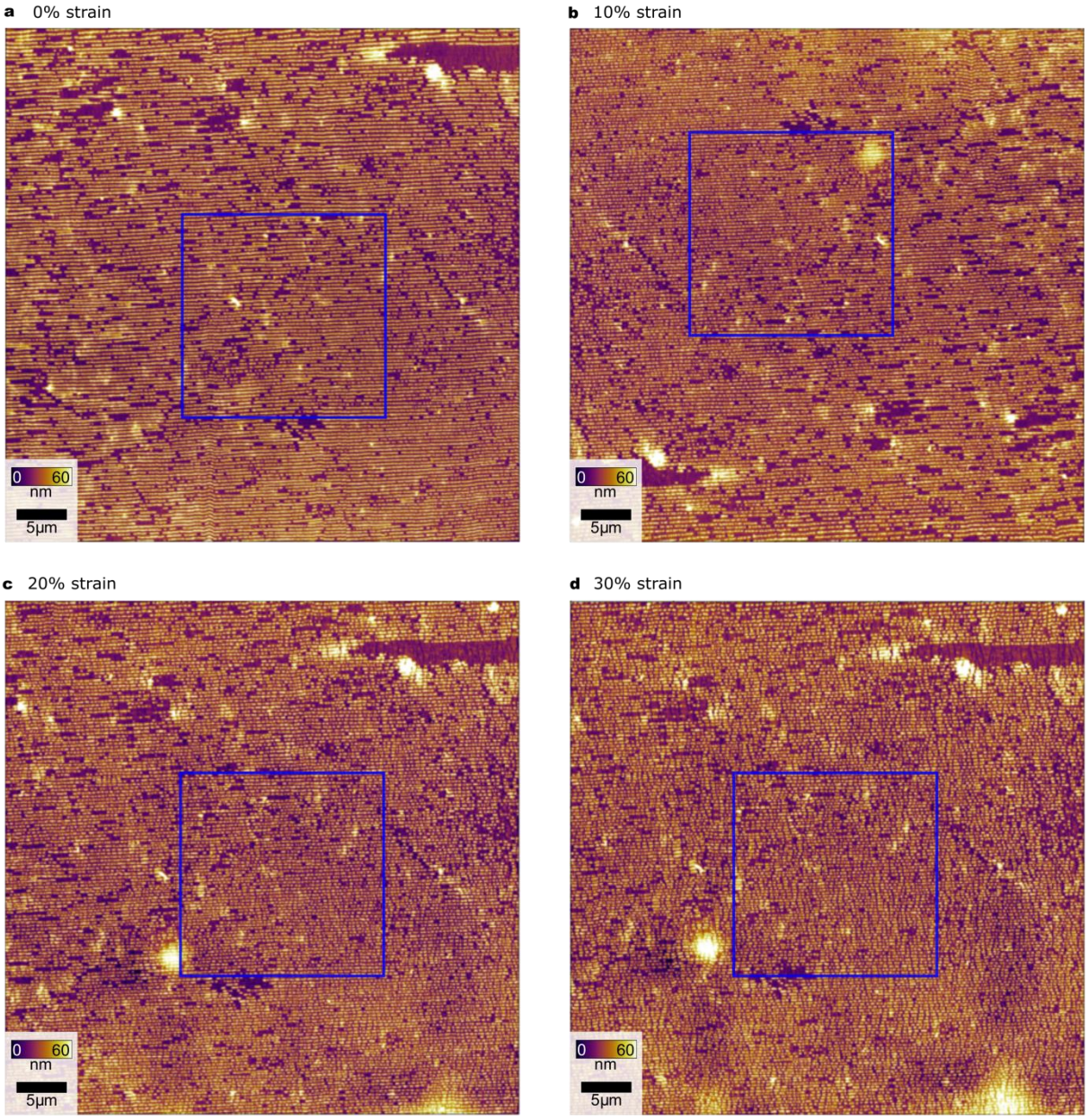

Figure S11: AFM overview images used to locate the same spot during *in-situ* measurements: Height images at strains of **(a),** 0% **(b),** 10% **(c),** 20% and **(d)** 30%**.**

AFM images were recorded on an MFP-3D Bio with the NanoRack™ stretching stage (Asylum Research, An Oxford Instrument Company, Santa Barbara, CA) in tapping mode™ using a cantilever with a nominal spring constant of 26 N/m (OTESPA-R3, $f_R \approx 300$ kHz, Bruker). The clamped ends of the PDMS strip were covered with Parafilm™ to reduce stress spikes from the clamps. The zero-strain condition of the sample was adjusted by eye and the initial length was determined with a caliper rule. To ensure that measurements at each strain were always conducted at the same position, the top-view optic of the AFM was used to locate the measuring spot on the microscopic scale. Immediately before imaging, the bottom

support of the NanoRack™ was lifted until it slightly touched the sample to ensure stable imaging conditions. First, 50 × 50 µm^2 overview images (**a–d**) were recorded to locate the desired measuring spot, followed by high-resolution (1024 lines, 2048 points/line) 20 × 20 µm^2 zoom-in images (**blue frame**). After imaging, the bottom support was removed, the strain was incremented (*i.e.*, to 10%, 20%, 30%), and the above-mentioned protocol was repeated.

The recorded AFM images were tilt-corrected by excluding all particles and performing the flatten function with the image analysis software from Asylum Research. Statistical evaluation of the assembly was performed with a homemade IgorPro 7 (Wavemetrics, USA) algorithm. First, binary masks were calculated in which the highest asperity position in each particle represents the center. This was achieved with a brute-force approach, with every *z*-value in the image matrix above a threshold being analyzed. Each line and column were treated separately. *E.g.,* one line is checked from left to right until the first value above the threshold is found. A lateral position in a line is considered as a possible particle maximum if its *z*-value exceeds that of adjacent values. This procedure is repeated for all rows and columns, also taking into account the respective upper and lower positions of all possible adjacent maxima within the matrix. The positions where maxima from line and column searches coincide are assumed to represent the centers of particles. In the case of high lateral resolution images, multiple maxima can be found on one single particle. To avoid these artifacts, we analyzed the surroundings of every local maximum for neighboring maxima within a search radius of 65 nm (5 nm less than the particle diameter; close contact conditions). The best-match maximum of each single particle is thus considered as the particle center and used for the statistical evaluation of the assemblies.

Two adjacent particles are considered to belong to the same oligomer if their center-to-center distance is below 150 nm. This value equates to approximately 4 particle radii (above the distance threshold[7] for strong plasmonic coupling) and the resolution of the AFM scanning image (20 × 20 µm^2, 2048 points/lines). First, one particle center is chosen and its radial surroundings are analyzed for neighboring particles within the cut-off distance. If a neighboring particle center is found within the search range, its lateral position is taken as the new search center. This procedure is continued until no new particles centers can be found within the search radius. The area occupied by one distinct oligomer is highlighted by color-coding based on chain length (see **Figure S8**).

After analysis of the complete image, the accuracy and validity of the resulting maps were verified by visual inspection of overlays of the AFM height image, calculated particle maxima, and the oligomers. This procedure is exemplified in **Figure S11**.

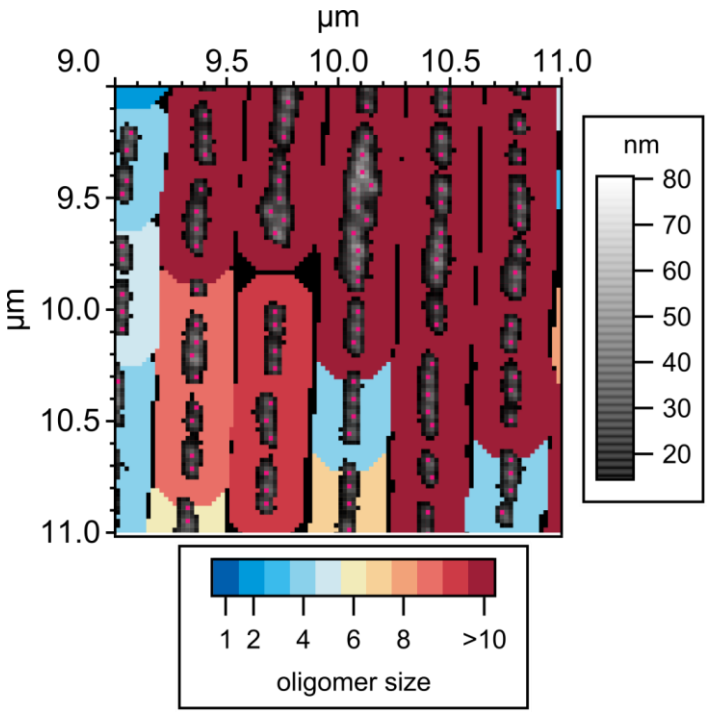

Figure S12: Exemplary analysis of AFM data for determination of oligomer length distribution. The final image is a superposition of the AFM height image (grayscale), the evaluated particle centers (pink dots), and the final analysis of the oligomer length color coded based on the number of particles per oligomer.

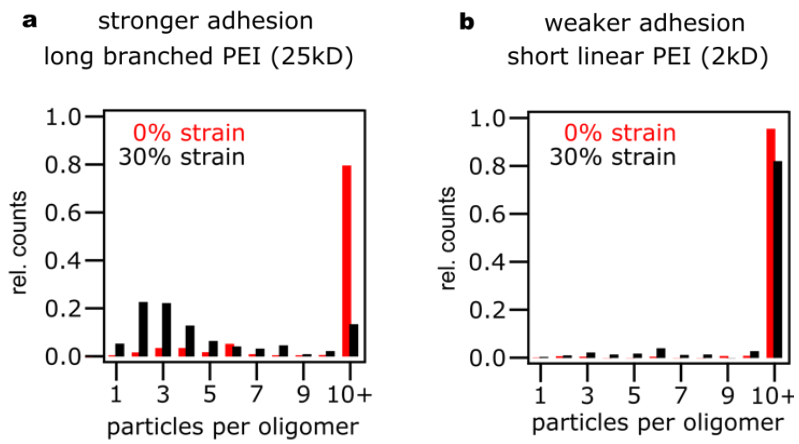

Figure S13: Control of the fragmentation process by adjusting the adhesion between particles and substrate. For a branched and high-molecular-weight PEI, fragmentation takes places indicating balanced interaction forces (**a**) For a linear and low-molecular-weight PEI, almost no fragmentation into oligomers can be observed (**b**). The different susceptibility for breakup is clearly visible in the normalized chain length distributions.

References

1. Buxton, G. A.; Care, C. M.; Cleaver, D.J., A Lattice Spring Model of Heterogeneous, Materials with Plasticity. *Modell. Simul. Mater. Sci. Eng.* **2001,** *9*, 485.
2. Persson, P.-O.; Strang, G., A Simple Mesh Generator in MATLAB. *SIAM review,* **2004,** *46,* 329-345.
3. Groot, R.D.; Warren, P.B., Dissipative particle dynamics: Bridging the Gap Between Atomistic and Mesoscopic Simulation. *J. Chem. Phys.* **1997,** *107,* 4423-4435.
4. Mayer, M.; Tebbe, M.; Kuttner, C.; Schnepf, M. J.; König, T. A. F.; Fery, A., Template-Assisted Colloidal Self-Assembly of Macroscopic Magnetic Metasurfaces. *Faraday Discuss.* **2016**, *191*, 159-176.
5. Hanske, C.; Tebbe, M.; Kuttner, C.; Bieber, V.; Tsukruk, V. V.; Chanana, M.; König, T. A. F.; Fery, A., Strongly Coupled Plasmonic Modes on Macroscopic Areas *via* Template-Assisted Colloidal Self-Assembly. *Nano Lett*. **2014**, *14*, 6863-6871.
6. Grushka, E., Characterization of Exponentially Modified Gaussian Peaks in Chromatography. *Anal. Chem.* **1972,** *44* , 1733-1738.
7. Myroshnychenko, V.; Rodríguez-Fernández, J.; Pastoriza-Santos, I.; Funston, A. M.; Novo, C.; Mulvaney, P.; Liz-Marzan, L. M.; García de Abajo, F. J., Modelling the Optical Response of Gold Nanoparticles. *Chem. Soc. Rev.* **2008**, *37,* 1792-1805.